A Full-Metal Dual-Band Millimeter-Wave Antenna Array With Concomitant Multifold Orthogonal Beamforming for V2V and V2I Communications

Zhonghe Zhang, Sai-Wai Wong, *Senior Member, IEEE*, Youquan Wen, Shu-Qing Zhang, *Student Member, IEEE*, Wenting Li, *Member, IEEE*, and Yejun He, *Senior Member, IEEE*

***Abstract*—This article introduces a millimeter-wave (mmWave) communication system with a concomitant multifold orthogonal beamforming (CMOB) antenna array to support vehicle-to-vehicle (V2V) and vehicle-to-infrastructure (V2I) communications. Through a single feed, the antenna triggers the TE_{011} and TE_{101} modes within the cavity, encompassing dual bands. Concurrently, it integrates slotted elements on various surfaces of the cavity to generate antenna beams distinguished by their orthogonal characteristics. A full-metal cavity provides high power handling capabilities without the need for complex feeding networks. For a 1×4 antenna array, we have employed three different designs: dual orthogonal beams, triple orthogonal beams, and quadruple orthogonal beams. This process is carried out to assess the viability of the designs and to fine-tune the shape of the quadruple orthogonal beams through optimization. Subsequently, a 1×4 antenna array featuring quadruple orthogonal beams is constructed and subjected to measurement. The gains of the array's orthogonal beams are 9.828 dBi and 9.655 dBi, which demonstrates a close correspondence with the simulated outcomes. This serves to affirm the practicality of the design approach.**

***Index Terms*—Concomitant multifold orthogonal beamforming (CMOB), dual-band, full metal antenna array, millimeter-wave, full-metal, vehicle-to-vehicle (V2V), vehicle-to-infrastructure (V2I).**

I. Introduction

WITH the rapid advancement of vehicle technology, high-speed communication in vehicles becomes paramount [1], [2], [3], [4], [5]. This trend is driving the emergence of various new application scenarios, including autonomous driving [6], cooperative perception [7], sensor data sharing [8], and multi-link communication [9]. Together, these innovations are enhancing both the safety and intelligence of driving.

Manuscript received 11 October 2023; revised 23 January 2024 and 27 February 2024; accepted 14 March 2024. Date of publication 19 March 2024; date of current version 16 July 2024. This work was supported in part by the National Key Research and Development Program of China under Grant 2023YFE0107900 and in part by the National Natural Science Foundation of China under Grant 62071306, Grant 62101341, and Grant 62171289. The review of this article was coordinated by Dr. Subhradeep Chakraborty. *(Corresponding authors: Sai-Wai Wong; Yejun He.)*

The authors are with the State Key Laboratory of Radio Frequency Heterogeneous Integration, Sino-British Antennas and Propagation Joint Laboratory of MOST, Guandong Engineering Research Center of Base Station Antennas and Propagation, Shenzhen Key Laboratory of Antennas and Propagation, College of Electronics and Information Engineering, Shenzhen University, Shenzhen 518060, China (e-mail: wongsaiwai@ieee.org; heyejun@126.com).

Digital Object Identifier 10.1109/TVT.2024.3378722

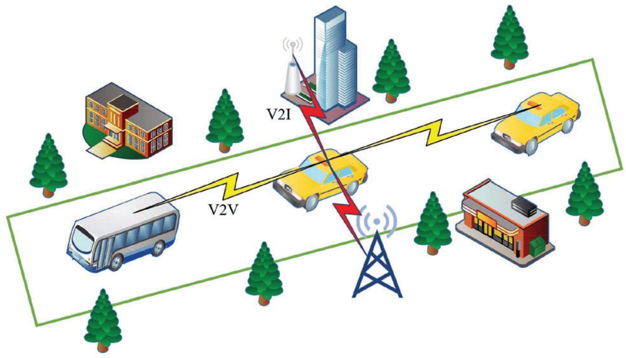

Fig. 1. Concomitant multifold orthogonal beamforming supporting both V2V and V2I.

In order to achieve Gbps vehicle communication, millimeter wave (mmWave) technology [10], [11], [12], [13], [14], [15] is considered as a highly promising option. Millimeter-wave technology possesses a wide spectrum availability, excellent reliable low-latency communication capabilities, and the ability to transmit large volumes of data. These features are expected to significantly enhance the resolution and precision of vehicle communication systems.

To ensure high-quality communication links supporting both vehicle to vehicle (V2V), vehicle to infrastructure (V2I) concurrently, as shown in Fig. 1, millimeter wave with high gain characteristics and multi-beam antenna technology is typically employed, enabling the switching of multiple beams while the vehicle is in motion [16]. Consequently, various multi-beam antenna technologies have been developed for this purpose, which can be achieved through multi-antenna systems [17], Butler matrix antennas [18], lenses [19], [20], transmit arrays [21], [22], leaky-wave antennas [23], and phased-array antennas [24]. All of these technologies are capable of generating multiple high-quality directional beams. However, due to their complex structures and large sizes, these technologies often face limitations in achieving a 90° scan from end-fire to broadside, and they cannot create concomitant orthogonal beams using simple feeding structure, which poses new challenges in the design of vehicle antennas.

Deploying multiple antennas in different directions is an effective approach to achieve orthogonal beams. The possibility

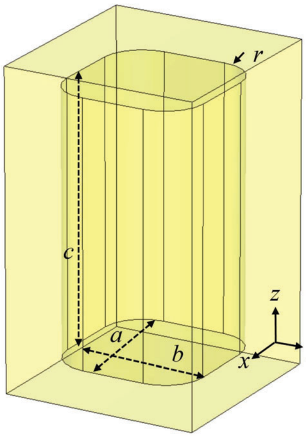

Fig. 2. Full metal cavity mode.

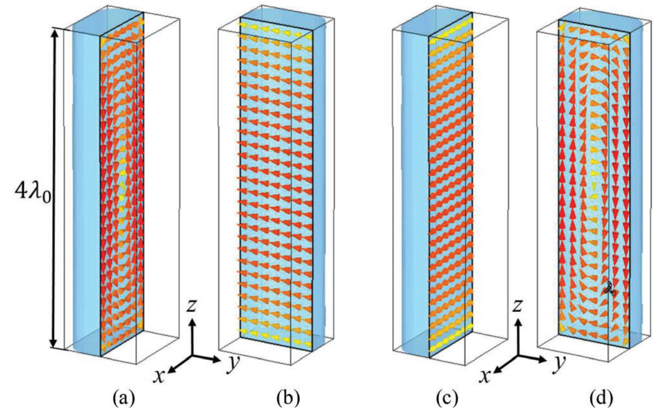

Fig. 3. EM field distributions of dual modes in a cavity resonator: (a) Magnetic field of TE_{101}, (b) electric field of TE_{101}, (c) electric field of TE_{011}, and (d) magnetic field of TE_{011}.

of using multi-directional beamforming antennas is realized by deploying three horn antennas in the end-fire directions and one horn antenna in the broadside direction [25]. Designing arrays in different directions can achieve high gain and wide beam coverage [26], [27], [28], but this occupies limited space. Using a shared-aperture approach resolved this issue [29], but complex feed networks and differing beam polarizations have limited the antenna's application in automobiles. The design and power distribution methods for a joint beamformer in an RF-VLCP [30] hybrid system have been proposed. In contrast to traditional patch antennas, full-metal structure antennas possess enhanced power handling capabilities. The simplicity of cavity resonance eliminates the need for complex feeding networks. Simultaneously, when combined with the concept of multidimensional radiation patterns, it facilitates multidirectional radiation within the millimeter-wave frequency range.

This paper introduces a full-metal dual-band millimeter wave antenna array with a single feed and no corporate feed network, enabling concomitant multifold orthogonal beamforming (CMOB) in dual bands to support V2V and V2I communications. Section II offers a concise explanation of the design principles. Section III focuses on the designs of concomitant dual orthogonal beamforming (CDOB) antenna array, concomitant triple orthogonal beamforming (CTOB) antenna array, and concomitant quadruple orthogonal beamforming (CQOB) antenna array, and optimizes the sidelobes and gain of the quadruple beam antenna array. The proposed antenna features concomitant multifold orthogonal beamforming, with advantages such as a simple structure, high efficiency, and high power-handling capability. In Section IV, the orthogonal 4-beam 1×4 antenna array is fabricated and measured to validate the design concept. Finally, Section V concludes this article.

II. Concept of Dual-Band Dual-Mode Resonance

This section commences by delving into the theoretical underpinnings of how a full-metal slot antenna achieves dual-band dual-mode orthogonal radiation. Fig. 2 exhibits a full-metal cavity model, where the cavity dimensions inside are specified as *a*, *b*, *c*, with the resonance frequencies of the proposed cavity expressed as

$$\omega_{mnl}^2 = \frac{\upsilon^2}{\mu_r \varepsilon_r}\left[\left(\frac{m\pi}{a}\right)^2 + \left(\frac{n\pi}{b}\right)^2 + \left(\frac{l\pi}{c}\right)^2\right] \tag{1}$$

where ω_{mnl} is the resonant frequency, and the modulus is *m*, *n*, *l*. ν is the speed of light in a vacuum. μ_r and ε_r are the permeability and dielectric constant, respectively. To enhance signal transmission capabilities, antenna gains are increased in both the x-axis and y-axis directions, with the cavity's height *c* set at $4\times\lambda_0$ to achieve an array of 4 antenna slots arrangement of orthogonal beams. Simultaneously, the excitation is applied to induce two orthogonal fundamental modes, TE_{101} and TE_{011}. In addition, by adjusting the lengths of *a* and *b* differently, these two modes are achieved at different frequencies. The resonant frequencies of the dual-mode are expressed as

$$\omega_{101}^2 = \frac{\upsilon^2}{\mu_r \varepsilon_r}\left[\left(\frac{\pi}{a}\right)^2 + \left(\frac{\pi}{c}\right)^2\right] \tag{2}$$

$$\omega_{011}^2 = \frac{\upsilon^2}{\mu_r \varepsilon_r}\left[\left(\frac{\pi}{b}\right)^2 + \left(\frac{\pi}{c}\right)^2\right] \tag{3}$$

The EM field distribution of the dual mode within a full metal cavity resonator is depicted in Fig. 3. These two modes do not resonate at the same frequency. Simultaneous dual-mode operation can be achieved by configuring the feeding slot appropriately.

Slots along the x-axis and y-axis within a full-metal resonant cavity enable concomitant multifold orthogonal beamforming through dual-mode orthogonal electric fields in a rectangular cavity, as depicted in Fig. 4.

The combination of different rectangular cavity dimensions e.g., *a*, *b*, *c*, as expressed in (1)–(3), allows the cavity to resonate simultaneously in the TE_{101} and TE_{011} modes. Multiple slots on the metal wall of this rectangular cavity will enhance the antenna's gain in specific directions, thereby improving signal transmission.

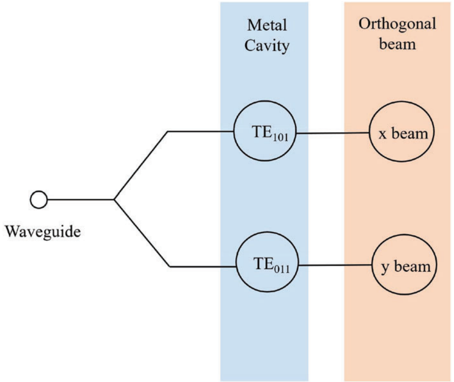

Fig. 4. Schematic diagram of dual-mode resonance for concomitant multifold orthogonal beamforming.

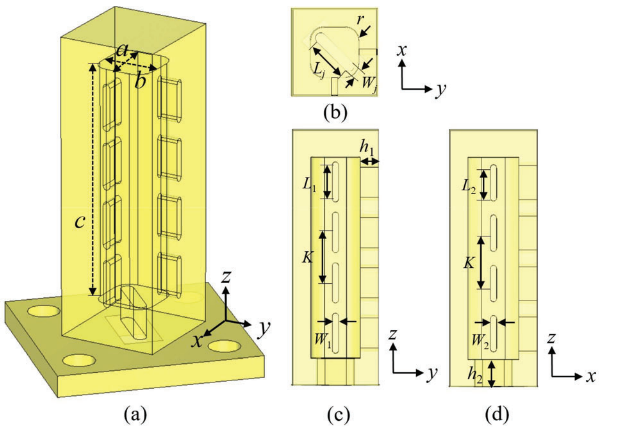

Fig. 5. Geometrical configuration of CDOB antenna array: (a) 3-D view, (b) top view, (c) front view, and (d) right view. Design parameters: $a = 5.6$, $b = 5.4$, $c = 22$, $L_j = 4.5$, $W_j = 1.2$, $h_1 = 2$, $h_2 = 3$, $L_1 = 3.7$, $W_1 = 0.7$, $L_2 = 3.3$, $W_2 = 0.7$, $k = 5.5$, $r = 1.3$ (unit: mm).

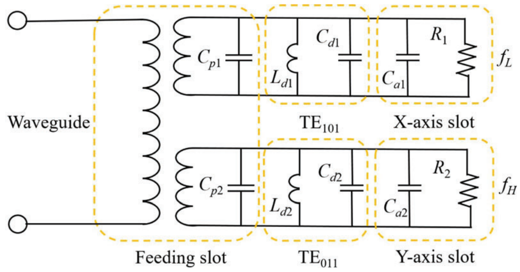

Fig. 6. Equivalent circuit model of the proposed dual-band antenna.

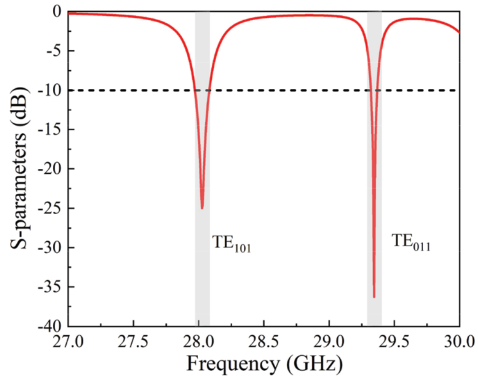

Fig. 7. Simulated return loss of the CDOB antenna array.

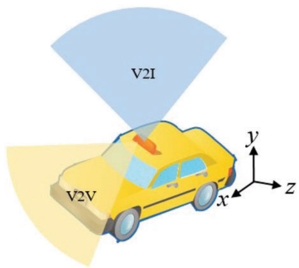

Fig. 8. Simultaneous CDOB antenna array radiation simulation on the vehicle.

III. Antenna Array Concomitant Multifold Orthogonal Beamforming Array Design

A. Concomitant Dual Orthogonal Beamforming Antenna

Fig. 5(a) illustrates the 3-D view of an antenna featuring a concomitant dual orthogonal beamforming (CDOB) antenna array, Fig. 5(b) provides a top view of the antenna, while Fig. 5(c) and Fig. 5(d) show the front and right views, respectively. The antenna is constructed as a rectangular full-metal structure and achieves radiation through waveguide slots feed from the bottom at a 45° rotation, which provides the x-axis and y-axis of electric field excitation simultaneously. Four equidistant and equally sized slots are positioned on both the front view and right view.

The antenna's equivalent circuit diagram is depicted in Fig. 6, with C_{p1} and C_{p2} denoting capacitive loads in different modes resulting from the rotational slot feeding, and C_{a1} and C_{a2} signifying capacitive loads in different modes arising from slot radiation. (L_{d1}, C_{d1}) represents the resonator model for the TE_{101} mode, while (L_{d2}, C_{d2}) characterizes the resonator model for the TE_{011} mode. Both modes coexist simultaneously without mutual interference due to the electric field orthogonal property, and the resonant frequencies of the two resonators can be determined using the following (4) and (5).

$$f_{101}^2 = \frac{1}{4\pi^2 L_{d1}^2 \left(C_{p1} + C_{d1} + C_{a1}\right)} \tag{4}$$

$$f_{011}^2 = \frac{1}{4\pi^2 L_{d2}^2 \left(C_{p2} + C_{d2} + C_{a2}\right)} \tag{5}$$

It is important that the structure of the reactive power division network reduces the complexity of the antenna, while the full-metal cavity enables a dual-band antenna array design with a small frequency ratio and orthogonal radiation properties. The frequency ratio of CDOB is 1.047.

Simulated antenna return loss is illustrated in Fig. 7, where the TE_{101} resonance mode is achieved at 28.03 GHz, and the TE_{011} resonance mode is attained at 29.34 GHz. The antenna radiates in both the +x and +y directions at two frequencies. Fig. 8 displays the antenna placement on the vehicle, enabling high-gain millimeter-wave radiation simultaneously in the end-fire and

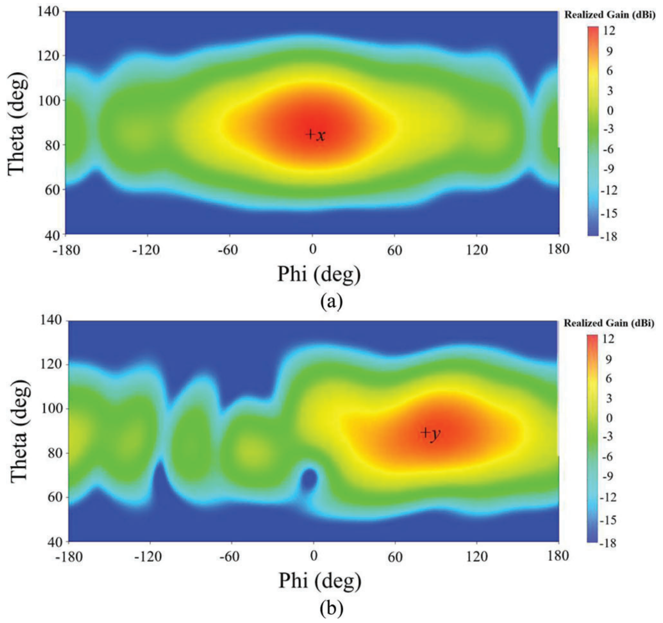

Fig. 9. Simulated contour plot of 3-D radiation patterns in different beam scanning angles at (a) 28.03 GHz and (b) 29.34 GHz.

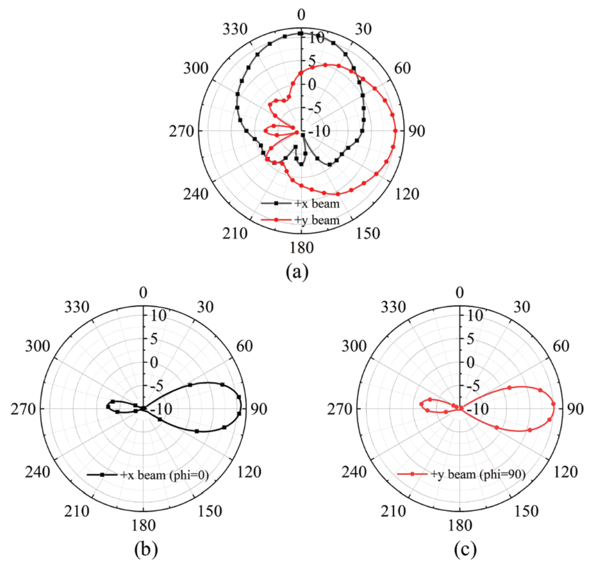

Fig. 10. Simulated radiation patterns of CDOB antenna array, (a) xy-plane, (b) xz-plane, and (c) yz-plane.

broadside directions. It provides concomitant communication links for both V2V and V2I.

The contour plot in Fig. 9 provides a visual representation of the 3-D radiation pattern, highlighting a noticeable 90° phase difference between the two radiation directions. The antenna realized gains of 10.89 dBi at 28.03 GHz and 10.1 dBi at 29.34 GHz. Fig. 10 illustrates the radiation pattern of the Concomitant Dual Orthogonal Beamforming (CDOB) antenna array. The black and red lines correspond to 28.03 GHz and 29.34 GHz, respectively. Fig. 10(a) shows the radiation pattern of two modes on the xy-plane, Fig. 10(b) depicts the radiation pattern at 28.03 GHz on the xz-plane at phi = 0°, and Fig. 10(c) represents the radiation pattern at 29.34 GHz on the yz-plane at phi = 90°.

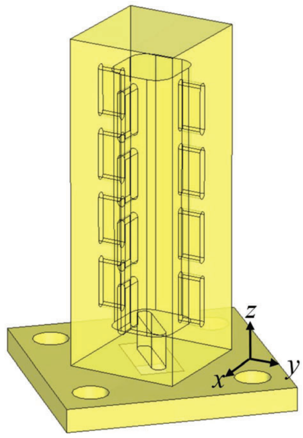

Fig. 11. Geometrical configuration of CTOB antenna array. Design parameters: $a = 5.6$, $b = 5.4$, $c = 22$, $L_j = 4.5$, $W_j = 1.2$, $h_1 = 2$, $h_2 = 3$, $L_1 = 3.8$, $W_1 = 0.7$, $L_2 = 3.4$, $W_2 = 0.7$, $k = 5.5$, $r = 1.3$ (unit: mm).

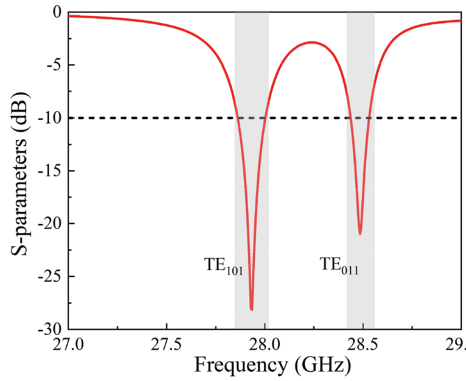

Fig. 12. Simulated return loss of the CTOB antenna array.

B. Concomitant Triple Orthogonal Beamforming Antenna Array

Fig. 11 illustrates the 3-D view of an antenna featuring a concomitant triple orthogonal beamforming (CTOB) antenna array, In the +x direction of the antenna, there are slots of equal size and spacing to achieve radiation at 27.93 GHz. What sets CDOB antenna array apart is that the CTOB antenna array has slots of the same size and spacing in both the +y and −y directions. The slot distribution is consistent on both faces, enabling dual-beam radiation at 28.47 GHz. The frequency ratio of CTOB is 1.019, the feeding slots are still rotated at 45 degrees to simultaneously excite two different modes.

The simulated concomitant triple orthogonal beamforming antenna array exhibits return loss as shown in Fig. 12. It achieves radiation in the TE_{101} mode at 27.93 GHz and in the TE_{011} mode at 28.47 GHz, with both modes exhibiting a return loss below −20 dB.

Fig. 13 displays the antenna placement on the vehicle, enabling high-gain millimeter-wave radiation simultaneously in the +x direction and in the +y and −y directions.

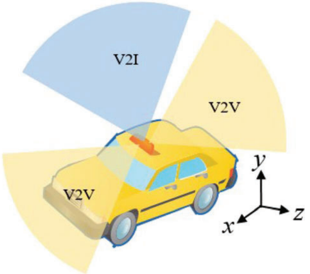

Fig. 13. Simultaneous CTOB antenna array radiation simulation on the vehicle.

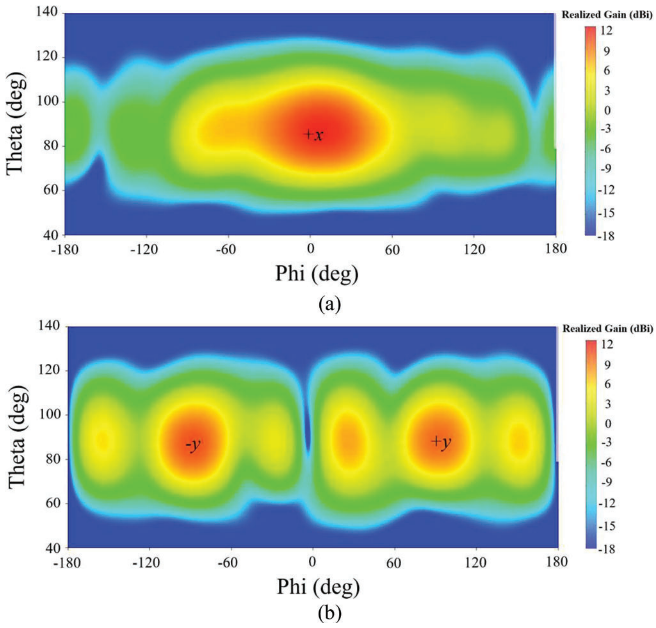

Fig. 14. Simulated contour plot of 3-D radiation patterns in different beam scanning angles at (a) 27.93 GHz and (b) 28.47 GHz.

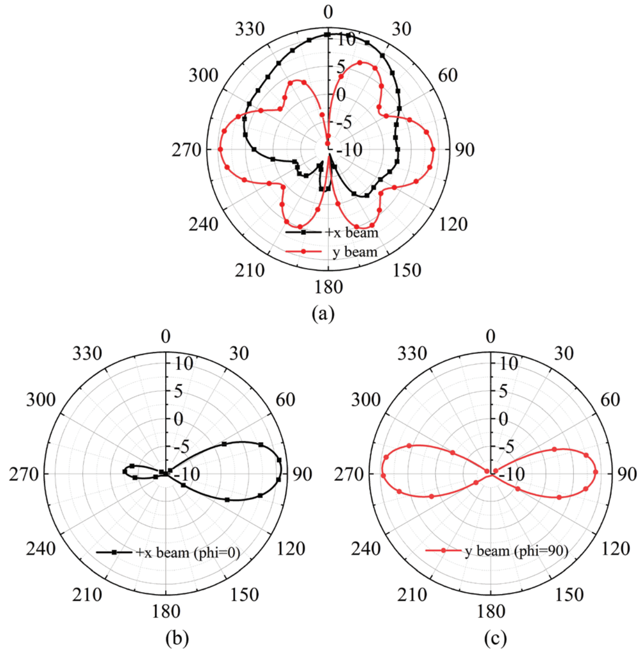

Fig. 15. Simulated radiation patterns of CTOB antenna array: (a) xy-plane, (b) xz-plane, and (c) yz-plane.

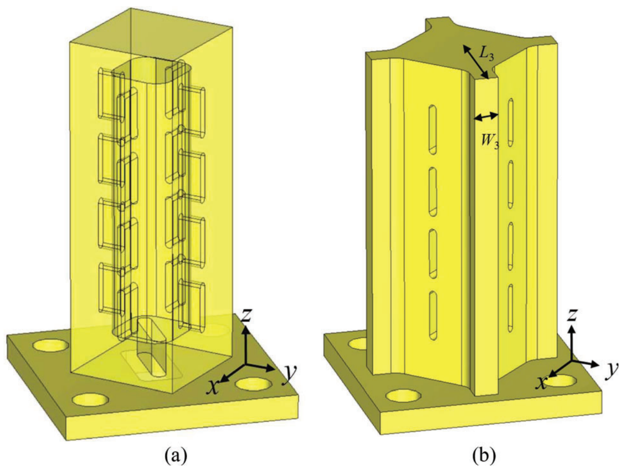

Fig. 16. Geometrical configuration of CQOB antenna array: (a) Initial configuration, (b) final configuration. Design parameters: $a = 5.6$, $b = 5.4$, $c = 22$, $L_j = 4.5$, $W_j = 1.2$, $h_1 = 2$, $h_2 = 3$, $L_1 = 3.68$, $W_1 = 0.7$, $L_2 = 3.56$, $W_2 = 0.7$, $k = 5.5$, $r = 1.3$, $L_3 = 8$, $W_3 = 2$ (unit: mm).

The contour plot in Fig. 14 provides a visual representation of the 3-D radiation pattern, achieving orthogonal radiation in the +x and y directions. The antenna realized gains of 11.02 dBi at 27.93 GHz and 9.689 dBi at 28.47 GHz. Fig. 15(a) shows the radiation pattern of two modes on the xy-plane, while Fig. 15(b) shows the radiation pattern at 27.93 GHz on the xz- plane at phi = 0°, and Fig. 15(c) shows the radiation pattern at 28.47 GHz on the yz-plane at phi = 90°.

C. Concomitant Quadruple Orthogonal Beamforming Antenna Array

Fig. 16(a) depicts a 3-D view of the co-located concomitant quadruple orthogonal beamforming (CQOB) antenna array. It features slots of the same size and spacing in both the front view and back view, as well as in the left view and right view.

Fig. 16(b) depicts the final structure of the antenna, with the design process to be provided later.

Fig. 17 illustrates the simulated return loss characteristics of the CQOB antenna array. It operates in the TE_{101} mode at 27.18 GHz and the TE_{011} mode at 28.25 GHz, with both modes showing return loss values below −20 dB. The frequency ratio of CQOB is 1.039.

Fig. 18 displays the antenna placement on the vehicle, enabling high-gain millimeter-wave radiation simultaneously in the x directions as well as in the y directions.

Fig. 19 introduces the simulated radiation patterns of the CQOB antenna array. The antenna exhibits excellent beamforming orthogonality but experiences higher side lobes due to the absence of a ground plane. In the x direction, the main lobe gain is 9.18 dBi, with side lobes only 2.8 dBi lower than the main

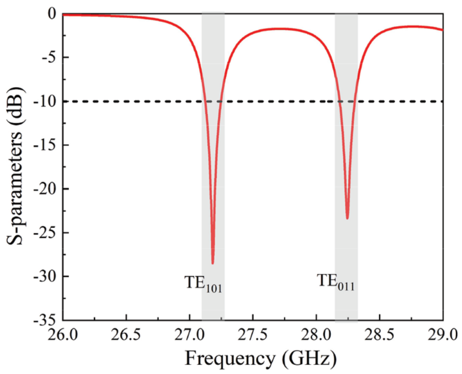

Fig. 17. Simulated return loss of the CTOB antenna array.

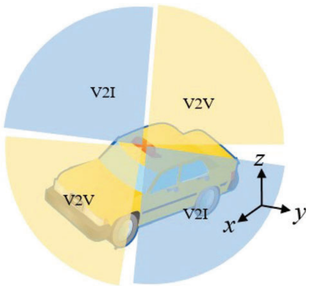

Fig. 18. Simultaneous CTOB antenna array radiation simulation on the vehicle.

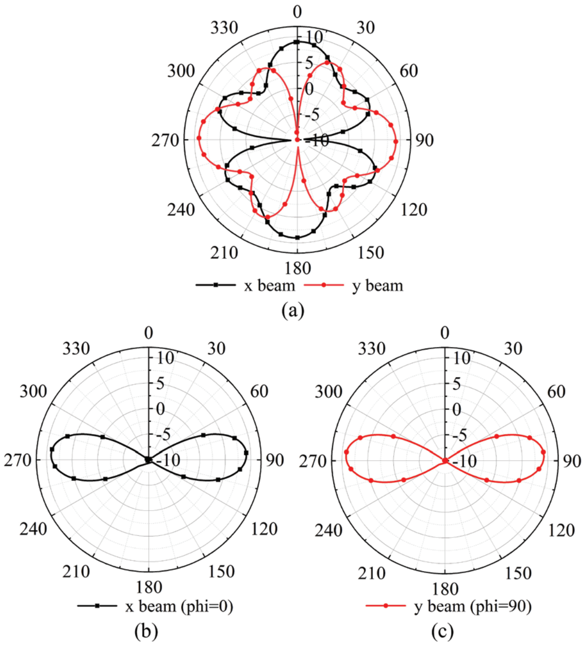

Fig. 19. Simulated radiation patterns of CQOB antenna array: (a) xy-plane, (b) xz-plane, and (c) yz-plane.

lobe. Similarly, in the y direction, the main lobe gain is 9.25 dBi, with side lobes 3.1 dBi lower than the main lobe.

The higher side lobe of the antenna is not suitable for antenna radiation. In order to address this issue, four branches are designed to reduce sidelobes in Fig. 16(b). These four branches

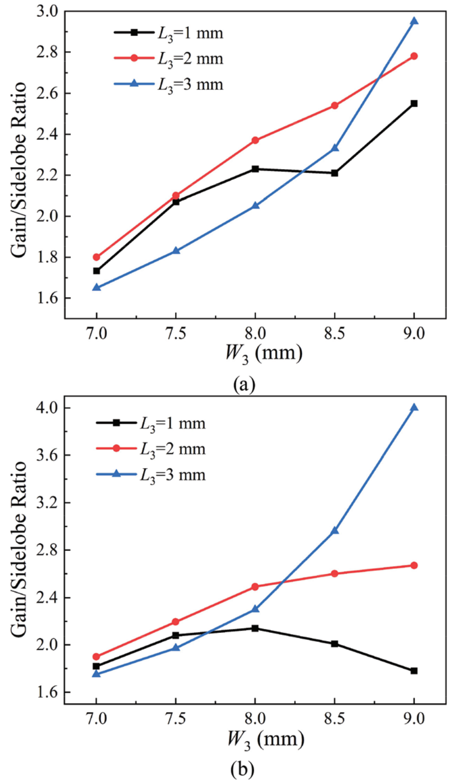

Fig. 20. Radiation parameter analysis of CQOB antenna array. (a) G/S ratio at 27.18 GHz in the x-axis, and (b) G/S ratio at 28.25 GHz in the y-axis.

are directly positioned at the four corners of the antenna, with a length of L_3 and a width of W_3.

To analyze the impact of these two parameters on the antenna's gain-to-sidelobe (G/S) ratio and main gain, as shown in Fig. 20(a) and (b), the addition of branches indeed reduces the antenna's G/S ratio. With the increase in W_3, there is a significant increase in the G/S ratio in both frequency bands. The peak gain of the antenna in two frequency bands is shown in Fig. 21(a) and (b). As W_3 increases, the antenna's peak gain will indeed decrease relative to the increase in antenna cost. Considering both the G/S ratio in two frequency bands and peak gain, the final design choice is $L_3 = 8$ and $W_3 = 2$ mm. Ultimately, the antenna simulation resulted in a radiation pattern with a peak gain of 10.2 dBi and a G/S ratio of 2.37 at 27.18 GHz. Similarly, at 28.25 GHz, it achieved a peak gain of 9.69 dBi and a G/S ratio of 2.49. The additional branches significantly improve the antenna radiation characteristics.

Without affecting the antenna impedance matching, the gain of the antenna is increased by 1.02 and 0.44 dBi at 27.18 GHz and 28.25 GHz, and the G/S ratio of the antenna is increased by 0.93 and 0.99 at 27.18 GHz and 28.25 GHz, respectively. Obviously, the external branch structure improves the radiation characteristics of the antenna. Finally, the full metal cavity structure provides support for the orthogonal beam requirement.

Fig. 22 presents a simulated contour plot of 3-D radiation patterns at different beam scanning angles at 27.18 and 28.25 GHz, providing dual-link communication for both V2V and V2I directions.

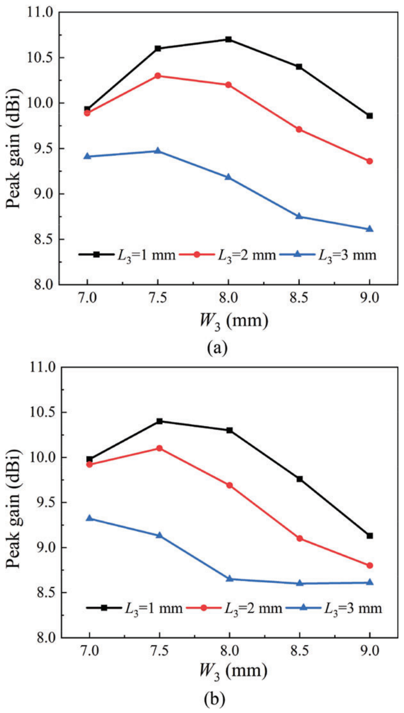

Fig. 21. Radiation parameter analysis of CQOB antenna array. (a) Peak gain at 27.18 GHz in the x-axis, and (b) peak gain at 28.25 GHz in the y-axis.

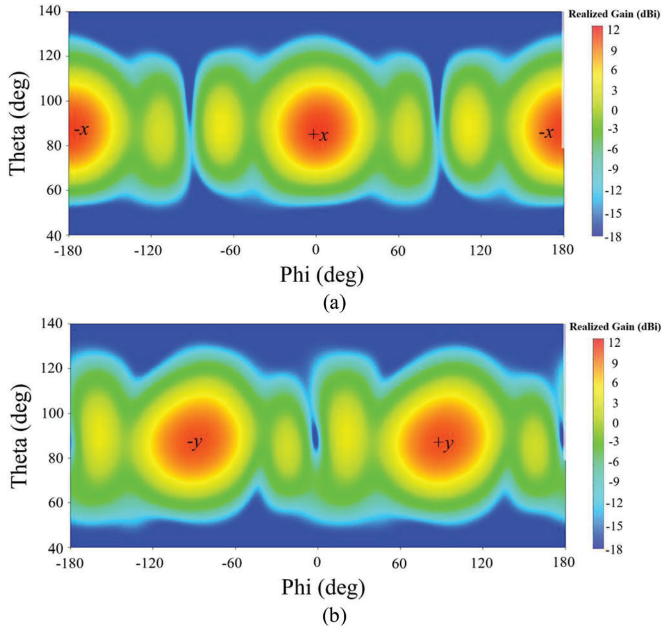

Fig. 22. Simulated contour plot of 3-D radiation patterns in different beam scanning angles at (a) 27.18 GHz and (b) 28.25 GHz.

IV. Experimental Results

To validate the concept of CMOB, the proposed 1×4 CQOB antenna array is manufactured using computer numerical control (CNC) machining and coated with gold-plated brass in Fig. 23. The comparison between simulated and measured $|S_{11}|$ and gain is shown in Fig. 24, and there is a high degree of agreement, with values below −20 dB at both 27.18 GHz and 28.25 GHz. The simulated and measured peak gains are consistent. It is worth mentioning that the directions corresponding to the two peak gains are different. At 27.18 GHz, the peak gain direction is in the +x and −x directions, while at 28.25 GHz, the peak gain direction is in the +y and −y directions.

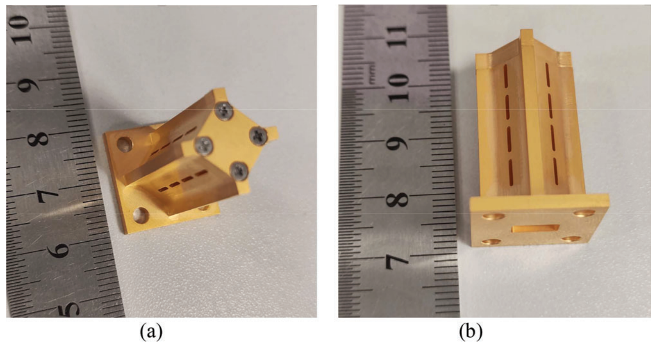

Fig. 23. Photographs of the proposed CQOB antenna array: (a) Top view, and (b) Side view.

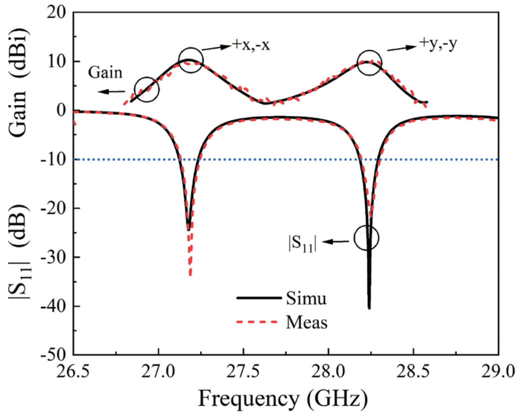

Fig. 24. Measured and simulated results of $|S_{11}|$ and gain.

The simulated and measured radiation patterns of the CQOB antenna array are shown in Fig. 25. At 27.18 GHz, the measured peak gain is 9.828 dBi, with the maximum gain direction in the +x and −x directions, and a G/S ratio of 2.52. Meanwhile, at 28.25 GHz, the measured peak gain is 9.655 dBi, with the maximum gain direction in the +y and −y directions, and a G/S ratio of 2.34. The differences between measured and simulated results are acceptable. The measured results verify the design of the paper. In both frequency bands, the simulated cross polarization is below −30 dBi, while the measured cross polarization at 27.18 GHz is below −13 dBi, and at 28.25 GHz, it is below −14 dBi. The cross-polarization of antenna measurement is higher than that of simulation because of the scattering of measurement environment.

V. Conclusion

A millimeter-wave array featuring concomitant multifold orthogonal beamforming is proposed, with the antenna excited in

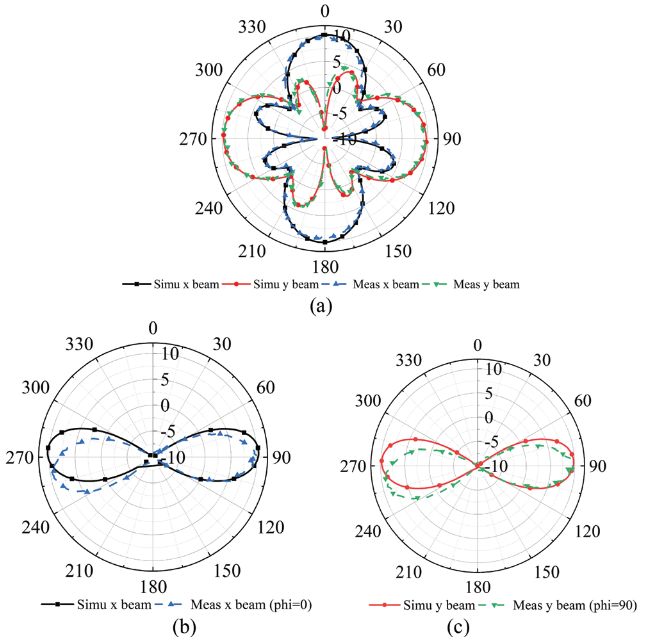

Fig. 25. Simulated and measured radiation patterns of CQOB antenna array, (a) xy-plane, (b) xz-plane, and (c) yz-plane.

two frequency bands by the TE_{101} and TE_{011} modes. These two modes excite beams with orthogonal properties. Following this principle, we designed 1×4 CDOB antenna array, 1×4 CTOB antenna array, and 1×4 CQOB antenna array, and conducted optimization on the radiation patterns of the 1×4 CQOB array. Measurements are conducted on the 1×4 CQOB array antenna to validate the design concept. This antenna array features concomitant multifold orthogonal beamforming, single-feed design, absence of power splitters, high gain, and high-power support. Simultaneously, it enables dual-link communication for V2V and V2I in orthogonality directions.

References

[1] R. I. Ansari et al., "5G D2D networks: Techniques, challenges, and future prospects," *IEEE Syst. J.*, vol. 12, no. 4, pp. 3970–3984, Dec. 2018.

[2] B. Ai, A. F. Molisch, M. Rupp, and Z.-D. Zhong, "5G key technologies for smart railways," *Proc. IEEE*, vol. 108, no. 6, pp. 856–893, Jun. 2020.

[3] M. Boban, A. Kousaridas, K. Manolakis, J. Eichinger, and W. Xu, "Connected roads of the future: Use cases, requirements, and design considerations for vehicle-to-everything communications," *IEEE Veh. Technol. Mag.*, vol. 13, no. 3, pp. 110–123, Sep. 2018.

[4] V. Va, J. Choi, T. Shimizu, G. Bansalet, and R. W. Heath Jr, "Inverse multipath fingerprinting for millimeter-wave V2I beam alignment," *IEEE Trans. Veh. Technol.*, vol. 67, no. 5, pp. 4042–4058, May 2018.

[5] R. He et al., "Propagation channels of 5G millimeter-wave vehicle-to-vehicle communications: Recent advances and future challenges," *IEEE Veh. Technol. Mag.*, vol. 15, no. 1, pp. 16–26, Mar. 2020.

[6] J. Chen, C. Zhang, J. Luo, J. Xie, and Y. Wan, "Driving maneuvers prediction-based autonomous driving control by deep Monte Carlo tree search," *IEEE Trans. Veh. Technol.*, vol. 69, no. 7, pp. 7146–7158, Jul. 2020.

[7] M. Koivisto, J. Talvitie, E. Rastorgueva-Foi, Y. Luo, and M. Valkama, "Channel parameter estimation and TX positioning with multi-beam fusion in 5G mmWave networks," *IEEE Trans. Wireless Commun.*, vol. 21, no. 5, pp. 3192–3207, May 2022.

[8] K. Zrar Ghafoor et al., "Millimeter-wave communication for internet of vehicles: Status, challenges, and perspectives," *IEEE Internet Things J.*, vol. 7, no. 9, pp. 8525–8546, Sep. 2020.

[9] M. Gapeyenko et al., "On the degree of multi-connectivity in 5G millimeter-wave cellular urban deployments," *IEEE Trans. Veh. Technol.*, vol. 68, no. 2, pp. 1973–1978, Feb. 2019.

[10] L. Chettri and R. Bera, "A comprehensive survey on Internet of Things (IoT) toward 5G wireless systems," *IEEE Internet Things J.*, vol. 7, no. 1, pp. 16–32, Jan. 2020.

[11] L. Zhang et al., "A survey on 5G millimeter wave communications for UAV-assisted wireless networks," *IEEE Access*, vol. 7, pp. 117460–117504, 2019.

[12] T. Bai and R. W. Heath, "Coverage and rate analysis for millimeter-wave cellular networks," *IEEE Trans. Wireless Commun.*, vol. 14, no. 2, pp. 1100–1114, Feb. 2015.

[13] T. S. Rappaport et al., "Millimeter wave mobile communications for 5G cellular: It will work!," *IEEE Access*, vol. 1, pp. 335–349, 2013.

[14] T. S. Rappaport, G. R. MacCartney, M. K. Samimi, and S. Sun, "Wideband millimeter-wave propagation measurements and channel models for future wireless communication system design," *IEEE Trans. Commun.*, vol. 63, no. 9, pp. 3029–3056, Sep. 2015.

[15] J. Zhang, S. Zhang, Z. Ying, A. S. Morris, and G. F. Pedersen, "Radiation-pattern reconfigurable phased array with pin diodes controlled for 5G mobile terminals," *IEEE Trans. Microw. Theory Techn.*, vol. 68, no. 3, pp. 1103–1117, Mar. 2020.

[16] E. T. Michailidis, N. Nomikos, P. Trakadas, and A. G. Kanatas, "Three-dimensional modeling of mmWave doubly massive MIMO aerial fading channels," *IEEE Trans. Veh. Technol.*, vol. 69, no. 2, pp. 1190–1202, Feb. 2020.

[17] Z. Chen, J. Tian, H. Liu, J. Yu, and X. Dong, "Novel pattern-diverse millimeter-wave antenna with broadband, high-gain, enhanced-coverage for energy-efficient unmanned aerial vehicle," *IEEE Trans. Veh. Technol.*, vol. 70, no. 5, pp. 4081–4087, May 2021.

[18] C. Ma, S. Y. Zheng, Y. M. Pan, and Z. Chen, "Millimeter-wave fully integrated dielectric resonator antenna and its multi-beam application," *IEEE Trans. Antennas Propag.*, vol. 70, no. 8, pp. 6571–6580, Aug. 2022.

[19] P. Liu, Y. Li, W. Cheng, X. Gao, and W. Zhang, "Multi-beam NOMA for millimeter-wave massive MIMO with lens antenna array," *IEEE Trans. Veh. Technol.*, vol. 69, no. 10, pp. 11570–11583, Oct. 2020.

[20] V. Basavarajappa, A. Pellon, I. Montesinos-Ortego, B. B. Exposito, L. Cabria, and J. Basterrechea, "Millimeter-wave multi-beam waveguide lens antenna," *IEEE Trans. Antennas Propag.*, vol. 67, no. 8, pp. 5646–5651, Aug. 2019.

[21] J. Hu, H. Wong, and L. Ge, "A circularly-polarized multi-beam magneto-electric dipole transmitarray with linearly-polarized feeds for millimeter-wave applications," *IEEE Trans. Antennas Propag.*, vol. 70, no. 7, pp. 6012–6017, Jul. 2022.

[22] L.-Z. Song, X. Wang, and P.-Y. Qin, "Single-feed multibeam conformal transmitarrays with phase and amplitude modulations," *IEEE Antennas Wireless Propag. Lett.*, vol. 21, no. 8, pp. 1669–1673, Aug. 2022.

[23] Y. Cao, S. Yan, J. Li, and J. Chen, "A pillbox-based dual circularly-polarized millimeter-wave multi-beam antenna for future vehicular radar applications," *IEEE Trans. Veh. Technol.*, vol. 71, no. 7, pp. 7095–7103, Jul. 2022.

[24] J. Y. Lee, J. Choi, D. Choi, Y. Youn, and W. Hong, "Broadband and wide-angle scanning capability in low-coupled mm-wave phased-arrays incorporating ILA with HIS fabricated on FR-4 PCB," *IEEE Trans. Veh. Technol.*, vol. 70, no. 3, pp. 2076–2088, Mar. 2021.

[25] N. Ojaroudiparchin, M. Shen, S. Zhang, and G. F. Pedersen, "A switchable 3-D-coverage-phased array antenna package for 5G mobile terminals," *IEEE Antennas Wireless Propag. Lett.*, vol. 15, pp. 1747–1750, Feb. 2016.

[26] H. Y. Kim, T. H. Jang, H. H. Bae, and G. S. Park, "A 60 GHz compact multidirectional-beam antenna-in-package for mobile devices," *IEEE Antennas Wireless Propag. Lett.*, vol. 18, no. 11, pp. 2434–2438, Nov. 2019.

[27] B. Sadhu et al., "A 250-mW 60-GHz CMOS transceiver SoC integrated with a four-element AiP providing broad angular link coverage," *IEEE J. Solid-State Circuits*, vol. 55, no. 6, pp. 1516–1529, Jun. 2020.

[28] J. Seo et al., "Miniaturized dual-band broadside/endfire antenna-in-package for 5G smartphone," *IEEE Trans. Antennas Propag.*, vol. 69, no. 12, pp. 8100–8114, Dec. 2021.

[29] B. Kim, M. Kim, D. Lee, J. Lee, Y. Youn, and W. Hong, "A shared-aperture cavity slot antenna-in-package concept featuring end-fire and broadside radiation for enhanced beam coverage of mmWave mobile devices," *IEEE Trans. Antennas Propag.*, vol. 71, no. 2, pp. 1378–1390, Feb. 2023.

[30] S. Shi, G. Gui, Y. Lin, C. Yuen, O. A. Dobre, and F. Adachi, "Joint beamformer design and power allocation method for hybrid RF-VLCP system," *IEEE Internet Things J.*, vol. 11, no. 5, pp. 7878–7892, Mar. 2024.

Zhonghe Zhang (Student Member, IEEE) was born in Jinzhong, Shanxi, China, in 1995. He received the B.S. and M.E. degrees from the North University of China, Taiyuan, China, in 2018 and 2021, respectively. He is currently working toward the Ph.D. degree with the College of Electronics and Information Engineering, Shenzhen University, Shenzhen, China. His current research interests include millimeter wave antennas and arrays, reconfigurable antennas and arrays, multibeam antennas and arrays.

Sai-Wai Wong (Senior Member, IEEE) received the B.S. degree in electronic engineering from the Hong Kong University of Science and Technology, Hong Kong, in 2003, and the M.Sc. and Ph.D. degrees in communication engineering from Nanyang Technological University, Singapore, in 2006 and 2009, respectively. From 2003 to 2005, he was an Electronic Engineer to lead an Electronic Engineering Department in China with two Hong Kong manufacturing companies. From 2009 to 2010, he was a Research Fellow with the ASTAR Institute for Infocomm Research, Singapore. Since 2010, he has been an Associate Professor and later become a Full Professor with the School of Electronic and Information Engineering, South China University of Technology, Guangzhou, China. Since 2017, he has been a tenured Full Professor with the College of Electronics and Information Engineering, Shenzhen University, Shenzhen, China. He has authored and coauthored more than 200 papers in international journals and conference proceedings. His current research interests include RF/microwave circuit and antenna design. He was the recipient of the New Century Excellent Talents in University awarded by the Ministry of Education of China in 2013 and the Shenzhen Overseas High-Caliber Personnel Level C in 2018.

Youquan Wen received the M.E. degree from Central South University, Hunan, China. He is currently working toward the Ph.D. degree with the College of Electronics and Information Engineering, Shenzhen University, Guangdong, China. His current research interests include radar cross section (RCS) reduction of antennas and metasurface, and magnetoelectric-dipole antenna/arrays.

Shu-Qing Zhang (Student Member, IEEE) was born in Jiangxi, China. He is currently working toward the master's degree with the College of Electronics and Information Engineering, Shenzhen University, Shenzhen, China. His current research interests include microwave filtering antenna, microwave circuits and 3D metal printing.

Wenting Li (Member, IEEE) received the B.S. degree in electronic information engineering and the M.S. degree in electromagnetic field and microwave technology from Northwestern Polytechnical University, Xi'an, China, in 2011 and 2014, respectively, and the Ph.D. degree in electronic engineering from University of Kent, Canterbury, U.K. in 2019. He is currently an Assistant Professor with the College of Electronics and Information Engineering, Shenzhen University, Shenzhen, China. His current research interests include reflectarray antennas, reconfigurable antennas, circularly polarized antennas, and multibeam antennas. Dr. Li was the recipient of the Shenzhen Overseas High-Caliber Personnel Level C ("Peacock Plan Award" C).

Yejun He (Senior Member, IEEE) received the Ph.D. degree in information and communication engineering from the Huazhong University of Science and Technology (HUST), Wuhan, China, in 2005. From 2005 to 2006, he was a Research Associate with the Department of Electronic and Information Engineering, The Hong Kong Polytechnic University, Hong Kong. From 2006 to 2007, he was a Research Associate with the Department of Electronic Engineering, Faculty of Engineering, The Chinese University of Hong Kong, Hong Kong. In 2012, he joined the Department of Electrical and Computer Engineering, University of Waterloo, Waterloo, ON, Canada, as a Visiting Professor. From 2013 to 2015, he was an Advanced Visiting Scholar (Visiting Professor) with the School of Electrical and Computer Engineering, Georgia Institute of Technology, Atlanta, GA, USA. From 2023 to 2024, he is an Advanced Research Scholar (Visiting Professor) with the Department of Electrical and Computer Engineering, National University of Singapore, Singapore.

Since 2006, he has been a Faculty of Shenzhen University, where he is currently a Full Professor with the College of Electronics and Information Engineering, Shenzhen University, Shenzhen, China, the Director of Sino-British Antennas and Propagation Joint Laboratory of Ministry of Science and Technology of the People's Republic of China (MOST), the Director of the Guangdong Engineering Research Center of Base Station Antennas and Propagation, and the Director of the Shenzhen Key Laboratory of Antennas and Propagation. He was selected as a Leading Talent in the "Guangdong Special Support Program" and the Shenzhen "Pengcheng Scholar" Distinguished Professor, China, in 2024 and 2020, respectively. He has authored or coauthored more than 300 refereed journal and conference papers and seven books. He holds about 20 patents. His research interests include wireless communications, antennas, and radio frequency.

Dr. He was also the recipient of the Shenzhen Overseas High-Caliber Personnel Level B (Peacock Plan Award B) and Shenzhen High-Level Professional Talent (Local Leading Talent). He was also the recipient of the Second Prize of Shenzhen Science and Technology Progress Award in 2017, Three Prize of Guangdong Provincial Science and Technology Progress Award in 2018, Second Prize of Guangdong Provincial Science and Technology Progress Award in 2023, and the 10th Guangdong Provincial Patent Excellence Award in 2023. He is currently the Chair of IEEE Antennas and Propagation Society-Shenzhen Chapter and obtained the 2022 IEEE APS Outstanding Chapter Award. Dr. He is a Fellow of IET, a Senior Member of the China Institute of Communications , and a Senior Member of the China Institute of Electronics. He was a Technical Program Committee Member or a Session Chair for various conferences, including the IEEE Global Telecommunications Conference (GLOBECOM), the IEEE International Conference on Communications (ICC), the IEEE Wireless Communication Networking Conference (WCNC), and the IEEE Vehicular Technology Conference (VTC). He served as the TPC Chair for IEEE ComComAp 2021 and the General Chair for IEEE ComComAp 2019. He was selected as a Board Member of the IEEE Wireless and Optical Communications Conference (WOCC). He was the TPC Co-Chair for WOCC 2023/2022/2019/2015, APCAP 2023, UCMMT 2023, ACES-China2023, NEMO 2020 and so on. He acted as the Publicity Chair of several international conferences such as the IEEE PIMRC 2012. He is serving as an Executive Chair of 2024 IEEE International Workshop of Radio Frequency and Antenna Technologies. He is the Principal Investigator for over 40 current or finished research projects, including the National Natural Science Foundation of China, the Science and Technology Program of Guangdong Province, and the Science and Technology Program of Shenzhen City. He was a Reviewer for various journals, such as the IEEE Transactions on Vehicular Technology, the IEEE Transactions on Communications, the IEEE Transactions on Industrial Electronics, the IEEE Transactions on Antennas and Propagation, the IEEE Wireless Communications, the IEEE Communications Letters. He is an Associate Editor for IEEE Transactions on Antennas and Propagation, IEEE Transactions on Mobile Computing, *IEEE Antennas and Propagation Magazine*, IEEE Antennas and Wireless Propagation Letters, *International Journal of Communication Systems, China Communications, ZTE Communications*.